

# Why Do Simple Molecules with “Isolated” Phenyl Rings Emit Visible Light?

Haoke Zhang,<sup>†,‡,§,Ⓛ</sup> Xiaoyan Zheng,<sup>†,‡</sup> Ni Xie,<sup>†,‡,§</sup> Zikai He,<sup>†,‡,§</sup> Junkai Liu,<sup>||</sup> Nelson L. C. Leung,<sup>†,‡,§,Ⓛ</sup> Yingli Niu,<sup>#</sup> Xuhui Huang,<sup>†,‡,Ⓛ</sup> Kam Sing Wong,<sup>⊥</sup> Ryan T. K. Kwok,<sup>†,‡,§,Ⓛ</sup> Herman H. Y. Sung,<sup>†</sup> Ian D. Williams,<sup>†</sup> Anjun Qin,<sup>||,Ⓛ</sup> Jacky W. Y. Lam,<sup>†,‡,§</sup> and Ben Zhong Tang<sup>\*,†,‡,§,||,Ⓛ</sup>

<sup>†</sup>Department of Chemistry, The Hong Kong University of Science and Technology, Clear Water Bay, Kowloon, Hong Kong, China

<sup>‡</sup>Hong Kong Branch of Chinese National Engineering Research Center for Tissue Restoration and Reconstruction, Institute for Advanced Study, Institute of Molecular Functional Materials, State Key Laboratory of Molecular Neuroscience, The Hong Kong University of Science and Technology, Clear Water Bay, Kowloon, Hong Kong, China

<sup>§</sup>Guangdong Provincial Key Laboratory of Brain Science, Disease and Drug Development, HKUST Shenzhen Research Institute, No. 9 Yuexing First RD, South Area, Hi-tech Park Nanshan, Shenzhen 518057, China

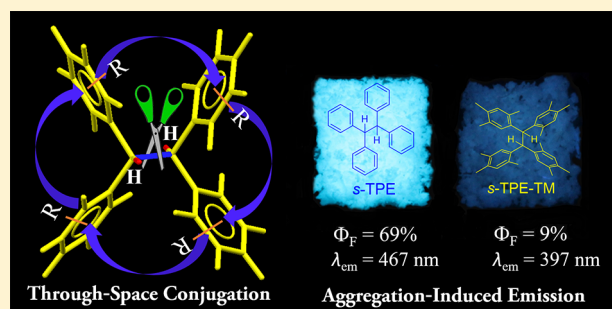
<sup>||</sup>Guangdong Innovative Research Team, SCUT-HKUST Joint Research Laboratory, State Key Laboratory of Luminescent Materials and Devices, South China University of Technology, Guangzhou 510640, China

<sup>⊥</sup>Department of Physics, The Hong Kong University of Science and Technology, Clear Water Bay, Kowloon, Hong Kong, China

<sup>#</sup>National Center for Nanoscience and Technology, Beijing 100190, China

## Supporting Information

**ABSTRACT:**  $\pi$ -Bonds connected with aromatic rings were generally believed as the standard structures for constructing highly efficient fluorophores. Materials without these typical structures, however, exhibited only low fluorescence quantum yields and emitted in the ultraviolet spectral region. In this work, three molecules, namely bis(2,4,5-trimethylphenyl)methane, 1,1,2,2-tetrakis(2,4,5-trimethylphenyl)ethane, and 1,1,2,2-tetra-phenylethane, with nonconjugated structures and isolated phenyl rings were synthesized and their photophysical properties were systematically investigated. Interestingly, the emission spectra of these three molecules could be well extended to 600 nm with high solid-state quantum yields of up to 70%. Experimental and theoretical analyses proved that intramolecular through-space conjugation between the “isolated” phenyl rings played an important role for this abnormal phenomenon.



## 1. INTRODUCTION

Fluorescence is a gift from nature and plays an important role in our colorful world. Inspired by nature, humanity started to study this “interesting phenomenon” in the early 19<sup>th</sup> century. Deeper cognition on the fluorescence process can not only reveal some natural laws but also better utilize and reform the natural world. Considered from the view of academic research, why a fluorophore emits light and how to design a highly efficient fluorophore are two important issues for scientists. With the rapid development of science and technology, fluorescence-based techniques have been well applied in the fields of biology,<sup>1</sup> medicine,<sup>2</sup> optoelectronics,<sup>3</sup> mechanical engineering,<sup>4</sup> and so forth, as evidence by the Nobel prize in Chemistry in 2008 and 2014 for the discovery of green fluorescent protein and super-resolved fluorescence microscopy, respectively.

Generally, fluorophores can be divided into organic and inorganic systems. Due to the good biocompatibility, adjust-

ability, and portability of organic fluorophores, many scientists have been attracted to work in this area. So far, most of the organic fluorophores are conjugated systems, with different emitting units linking together by double bonds, triple bonds, heteroatoms, and aromatic rings.<sup>5</sup> However, there are some special species which do not contain any of the above linkers in their structures but still show visible fluorescent emission. Representative examples are given by biological systems,<sup>6</sup> artificial polymers like poly(*N*-vinyl carbazole)<sup>7</sup> and polystyrene,<sup>8</sup> and peptide,<sup>9</sup> whose emissions have been observed for a long time but the associated mechanisms are still unclear and hard to explain with the traditional photophysical theories. Thus, the development of new reliable models to explain these abnormal phenomena is needed and will be of academic importance.

Received: August 12, 2017

Published: October 24, 2017

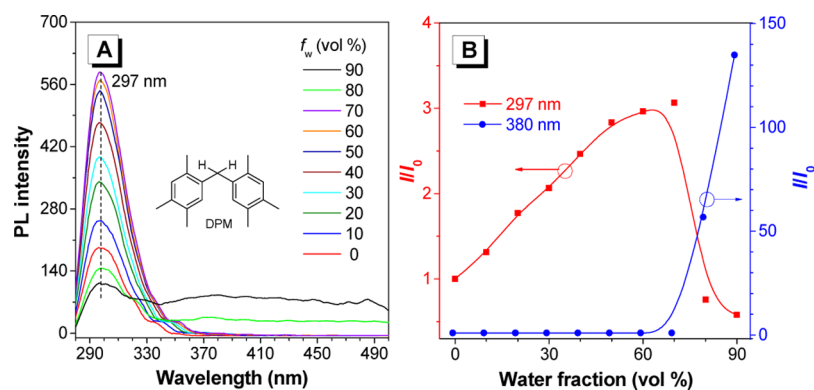


**Figure 1.** (A) PL spectra of DPM in THF/water mixture with different water fractions ( $f_w$ ). (B) Plots of relative PL intensity ( $I/I_0$ ) versus  $f_w$  at different emission wavelengths. Concentration =  $10^{-4}$  M,  $\lambda_{\text{ex}} = 280$  nm,  $I_0 =$  intensity at  $f_w = 0\%$ .

**Table 1. Photophysical Properties of DPM, *s*-TPE-TM, and *s*-TPE<sup>a</sup>**

compound	$\lambda_{\text{abs}}$ (nm)	fluorescence			$\Phi_{\text{F,solid}}$ (%)
		$\lambda_{\text{em, soln}}$ (nm)	$\lambda_{\text{em, agr}}$ (nm)	$\lambda_{\text{em, solid}}$ (nm)	
DPM	278	297	297, ~400	400	2
<i>s</i> -TPE-TM	280	300	305, 385	397	9
<i>s</i> -TPE	270	290	310, 460	467	69

<sup>a</sup>Abbreviation:  $\lambda_{\text{abs}}$  = absorption maximum in THF solution,  $\lambda_{\text{em, soln}}$  = emission maximum in THF solution,  $\lambda_{\text{em, agr}}$  = emission maximum in THF/water (1:9, v/v),  $\lambda_{\text{em, solid}}$  = emission maximum in solid powder,  $\Phi_{\text{F, solid}}$  = fluorescence quantum yield of solid powder measured by an integrating sphere.

So far, it is believed that the development of highly efficient fluorophores relies largely on high electronic conjugation. However, the biocompatibility and processability of these materials are of concern when they are utilized in biological applications. However, nonconjugated systems, such as some natural materials, possess high molecular flexibility, biocompatibility, and processability. Thus, if they can be designed to own visible range emission and high fluorescence quantum yield, a new research area will be opened. Actually, some published papers have already shown us some inspiring results. For example, Hirayama found that diphenyl- and triphenyl-alkanes showed longer-wavelength emission at around 330 nm and attributed such phenomenon as intramolecular excimer formation.<sup>10</sup> At the same time, isotactic polystyrene was discovered to exhibit a similar fluorescent property by Lumry et al.<sup>8</sup> However, in this system, the emission was located in the invisible range with a low fluorescence quantum yield. Thus, this work had attracted little attention. Traditionally, excimer formation was generally considered as the reason for fluorescence quenching. Thus, luminogens are often designed to avoid the excimer formation.<sup>11</sup> Recently, many systems proved that excimers could enhance and bathochromically shift the emission depending on the packing structure.<sup>12,13</sup> Thus, one question arises: is it possible to construct efficient nonconjugated luminogens with high quantum yield and visible emission?

In this work, three nonconjugated compounds, namely bis(2,4,5-trimethylphenyl)methane (DPM), 1,1,2,2-tetrakis(2,4,5-trimethylphenyl)ethane (*s*-TPE-TM), and 1,1,2,2-tetraphenylethane (*s*-TPE) with isolated phenyl rings were synthesized according to Scheme S1 in Supporting Information (SI) and characterized satisfactorily by standard spectroscopic methods (Figures S1–S4). Their photophysical properties were studied. Results showed that *s*-TPE showed high fluorescence quantum yield of ~70% and longer-wavelength emission at

~470 nm. The intramolecular through-space conjugation was found to play a major role rather than the  $\pi$ -electronic conjugation in the visible emission. Meanwhile, the restriction of the intramolecular motions (RIM),<sup>14,15</sup> which served as a mechanism of the aggregation-induced emission (AIE) phenomenon,<sup>16,17</sup> helped to convert the harmful effect of excimer formation on the light emission process into a constructive one.

## 2. RESULTS AND DISCUSSION

**2.1. Aggregation-Induced Emission.** Generally, most of the AIE luminogens (AIEgens) possess propeller-like structures, and the free motion such as rotation and vibration of each subunit will lead to the loss of excited state energy in a nonradiative decay manner to quench the fluorescent emission in solution. When aggregates form, such molecular motion will be restricted to block the nonradiative decay pathways. Alternatively, the radiative decay will dominate the photophysical process to enable the AIEgens to show strong emission in the aggregate state. Inspired by the fluorescence of homopolymer and copolymer of styrene, DPM was synthesized, in which two substituted phenyl rings were bridged by a methylene group (Figure 1A). Figure S5A showed its UV spectrum in THF/water mixture. The absorption maximum ( $\lambda_{\text{abs}}$ ) was located at 278 nm in both solution and aggregate states, and was almost identical to that of 1,2,4-trimethylbenzene ( $\lambda_{\text{abs}} \approx 277$  nm).<sup>18</sup> Its photoluminescence (PL) spectrum in pure THF (Figure 1A) was peaked at 297 nm associated with the emission of individual phenyl ring.<sup>19</sup> The emission became stronger upon gradual addition of water into the THF solution but decreased when the water fraction ( $f_w$ ) exceeded 70%. Meanwhile, a new broad peak arose from 350 to 500 nm, which intensified with increasing  $f_w$ . At 90% water fraction, the PL intensity at 380 nm was 140 times higher than that in pure THF solution (Figure 1B).<sup>20</sup> Since aggregates of DPM should

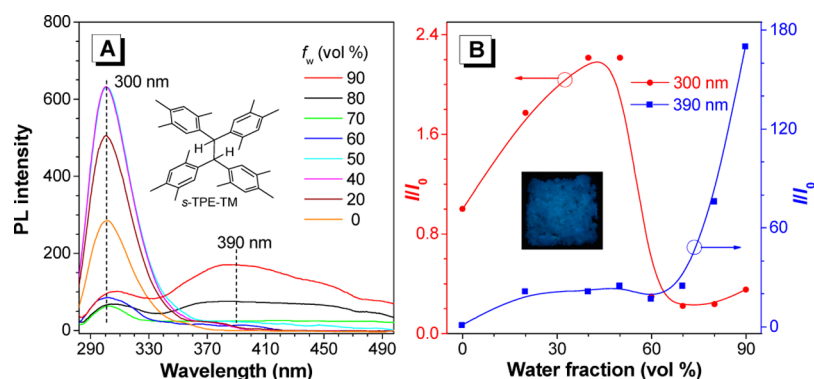


**Figure 2.** (A) PL spectra of *s*-TPE-TM in THF/water mixture with different water fractions ( $f_w$ ). (B) Plots of relative PL intensity ( $I/I_0$ ) versus  $f_w$  at different emission wavelengths. Concentration =  $10^{-4}$  M,  $\lambda_{\text{ex}} = 280$  nm,  $I_0$  = intensity at  $f_w = 0\%$ . Inset: fluorescent photos of *s*-TPE-TM solid taken under 365 nm UV light irradiation.

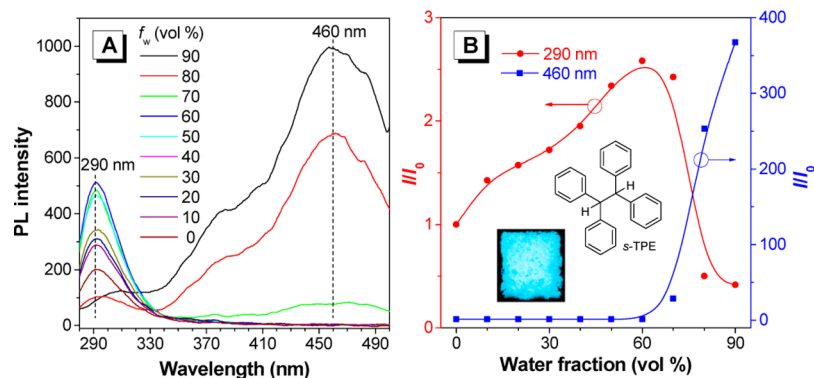


**Figure 3.** (A) PL spectra of *s*-TPE in THF/water mixture with different water fractions ( $f_w$ ). (B) Plots of relative PL intensity ( $I/I_0$ ) versus  $f_w$  at different emission wavelengths. Concentration =  $10^{-4}$  M,  $\lambda_{\text{ex}} = 280$  nm,  $I_0$  = intensity at  $f_w = 0\%$ . Inset: fluorescent photos of *s*-TPE solid taken under 365 nm UV light irradiation.

be readily formed in the presence of such a large amount of water, this suggests that the longer-wavelength emission demonstrates an AIE phenomenon. In the solid state, DPM showed an emission peak at 400 nm and its PL spectrum was well extended to 600 nm (Figure S6 and Table 1).

Although visible emission was observed in DPM, the associated fluorescence quantum yield ( $\Phi_F$ ) was quite low, and was measured to be merely 2%. We then studied the light-emitting property of *s*-TPE-TM, which could be regarded as dimer of DPM (Figure 2A). Its higher molecular rigidity is expected endow it with a higher  $\Phi_F$ . Its absorption maximum was located at 280 nm and was similar to 1,2,4-trimethylbenzene (Figure S5B). It showed an emission behavior resembling that of DPM (Figure 2). In the THF/water mixture with low water fraction, it exhibited only one peak at 300 nm. Again, a new broad peak appeared at 390 nm when  $f_w > 70\%$ . The intensity of the shorter-wavelength peak increased gradually when the  $f_w$  increased from 0% to 50%, but decreased afterward. However, the emission band at the longer wavelength was intensified progressively with increasing the water fraction. The maximum intensity enhancement was 170-fold. Like DPM, *s*-TPE-TM emitted at 397 nm in the solid state (Figure S6) but showed a higher  $\Phi_F$  of 9% (Table 1).

Traditional theories teach us that the intermolecular  $\pi$ - $\pi$  interaction is one of the causes for the aggregation-caused quenching effect.<sup>11</sup> However, some recent studies show that inter- or intramolecular  $\pi$ - $\pi$  interaction can result in fluorescence enhancement once aggregates form.<sup>21,22</sup> However,

the underlying reasons and theories are under strong debate as such a phenomenon was only observed in molecules with specific structures. To have a thorough conception and understanding of the photophysical properties of tetraphenyl-ethane system, the PL of *s*-TPE was further investigated (Figure 3B). The absorption maximum of *s*-TPE was 10 nm hypsochromic shift from that of *s*-TPE-TM and was located at 270 nm (Figure S5C). This may due to the absence of hyperconjugation between the benzene ring and the methyl groups.<sup>19,23,24</sup> Figure 3A showed that the PL spectrum in THF/water mixture with low water fraction exhibited only a peak at 290 nm assigned to benzene emission.<sup>19</sup> Similar to the above two compounds, the intensity of this shorter-wavelength peak increased first with increasing water fraction and then decreased afterward. Once aggregates formed at  $f_w > 60\%$ , a marvelous longer-wavelength emission at 460 nm was observed. This peak was intensified when more water was added and the maximum emission enhancement could reach 400-fold. In the solid state, a bright and sky blue fluorescence was observed under 365 nm UV light irradiation (Figure 3B inset). The emission peak was broad spanning from 400 to 600 nm with its maximum at 467 nm (Figure S6). The quantum yield was measured to be 70%, which subverted our traditional views to this kind of nonconjugated molecules (Table 1).

The PL analysis of all the molecules suggested that they possessed similar photophysical properties, and the longer-wavelength emission showed typical AIE effect. The intensity of the shorter-wavelength emission at around 300 nm increased

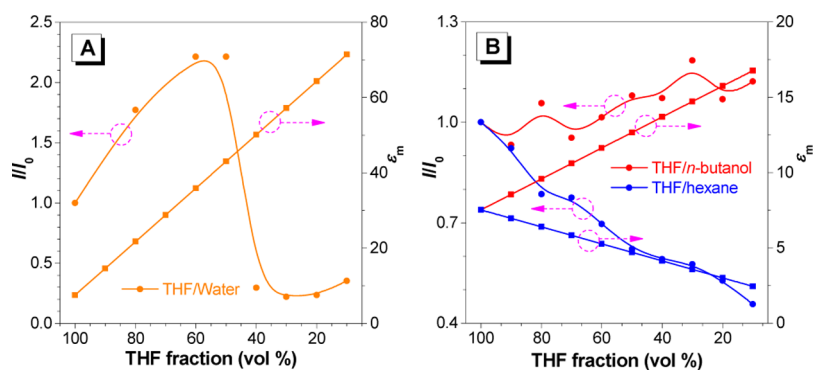


**Figure 4.** Plots of relative PL intensity ( $I/I_0$ ) and dielectric constant ( $\epsilon_m$ ) versus THF fraction ( $f_T$ ) of *s*-TPE-TM in (A) THF/water and (B) THF/*n*-butanol and THF/hexane mixtures. Concentration =  $10^{-4}$  M,  $\lambda_{ex}$  = 280 nm,  $I_0$  = intensity at  $f_T$  = 100%.

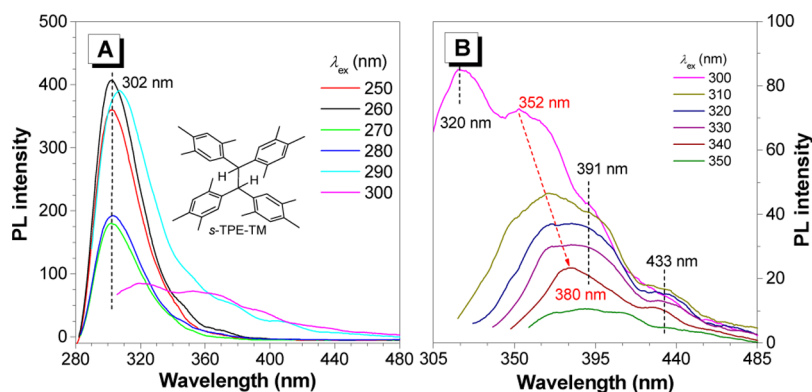


**Figure 5.** PL spectra of *s*-TPE-TM in THF solution ( $10^{-3}$  M) at different excitation wavelengths. (A) 250–300 nm and (B) 300–350 nm.

when the  $f_w$  in THF/water mixture rose from 0 to 60% and then decreased once aggregates formed. Such intensity annihilation should be ascribed to the energy transfer to longer-wavelength emissive species. However, the intensity of the shorter-wavelength emission peak increases from  $f_w = 0$  to  $\sim 60\%$  should have no relationship with the aggregate formation. Previous studies had shown that the molecular fluorescence was sensitive to the solvent polarity.<sup>25</sup> Thus, the PL spectra of *s*-TPE-TM in THF/hexane and THF/*n*-butanol mixtures were also measured and compared (Figures S7 and S8). Figure 4 showed the relationship between the relative emission intensity ( $I/I_0$ ) and dielectric constant ( $\epsilon_m$ ) of the mixed-solvent (Table S1). By lowering the THF fraction ( $f_T$ ) in THF/water mixture from 100 to 50%, the  $\epsilon_m$  increased from 7.520 to 43.030 accompanying with an increased  $I/I_0$  value to 2.3. Under the same  $f_T$  change,  $\epsilon_m$  of THF/*n*-butanol mixture increased from 7.520 to 16.772 along with an increase in  $I/I_0$  ratio to 1.2. However, the  $\epsilon_m$  of THF/hexane mixture decreased to 2.453 at  $f_T = 10\%$ , decreasing the  $I/I_0$  value to 0.5. Compared with water, *s*-TPE-TM could be solubilized in hexane and *n*-butanol in a certain amount. Thus, the aggregation-induced longer-wavelength emission was hard to observe in THF/hexane and THF/*n*-butanol mixtures and the plots of  $I/I_0$  versus  $f_T$  in Figure 4B were nearly linear. These data supported that the change of fluorescence intensity in solution was polarity-dependent, and the increase of mixed-solvent polarity resulted in the enhancement of emission intensity and vice versus.

**2.2. Excitation-Dependent Emission.** The dependence of PL of the present compounds on the excitation wavelength ( $\lambda_{ex}$ ) was examined. Figure S9 showed the PL spectra of DPM

in dilute THF (1 mM) obtained at different  $\lambda_{ex}$ . At  $\lambda_{ex}$  of 250–290 nm, only a single peak at 297 nm was observed. However, a longer-wavelength and weak emission appeared at 370 nm when the  $\lambda_{ex}$  increased to 310 nm. This peak red-shifted slightly, and its intensity decreased slowly by gradual varying the  $\lambda_{ex}$  from 310 to 360 nm. Figure 5 depicted that more than one peak was observed in *s*-TPE-TM at higher  $\lambda_{ex}$ . For example, four peaks at 320, 352, 391, and 433 nm were observed at  $\lambda_{ex} = 300$  nm. The peak at 352 nm “bathochromically shifted” to 380 nm when the  $\lambda_{ex}$  increased to 340 nm. The emission behaviors of *s*-TPE are similar to DPM and *s*-TPE-TM. Two peaks at 370 and 464 nm were observed when *s*-TPE was photoexcited at  $\lambda_{ex}$  of longer than 300 nm (Figure S10).

According to the traditional photophysical theory, variation in excitation could change only the emission intensity but not the wavelength of luminophores, especially for those with conjugated planar structures, such as pyrene and perylene.<sup>26</sup> The effect of excitation-dependent emission has already been observed and reported in other systems<sup>27,28</sup> and was ascribed to the mechanism of anti-Kasha’s rule in some case.<sup>29</sup> However, our AIEgens possess propeller-like structures. The free rotation of each group in solution will result in different conformations and each conformer show different electronic energy levels. The calculation of emission of all conformers formed a broad emission spectrum without any fine structure. With the increase in excitation wavelength or decrease in excitation energy, the number of excited conformers will decrease as the only species with low electronic energy gap will be excited. Thus, apparent “bathochromic shift” in the emission wavelength was observed and was due to a mathematical rather than a photophysical effect. Structure analysis of the molecules present in this work

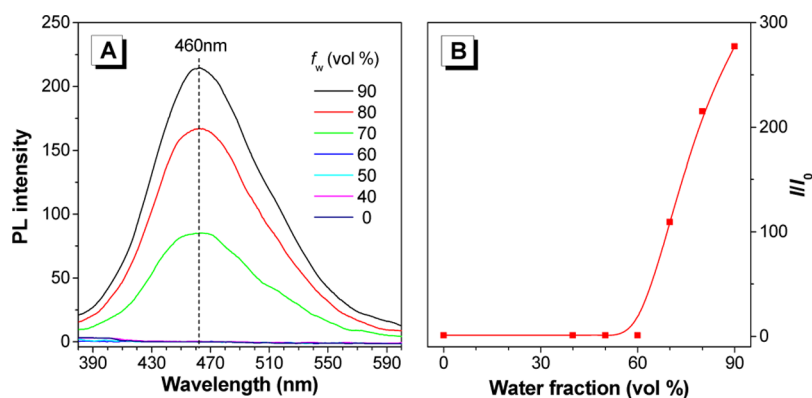


**Figure 6.** (A) PL spectra of *s*-TPE in THF/water mixtures with different water fractions ( $f_w$ ). Solution concentration = 100  $\mu$ M,  $\lambda_{ex}$  = 340 nm. (B) Plot of relative PL intensity ( $I/I_0$ ) versus  $f_w$  at 460 nm.  $I_0$  = fluorescence intensity at  $f_w$  = 0%.

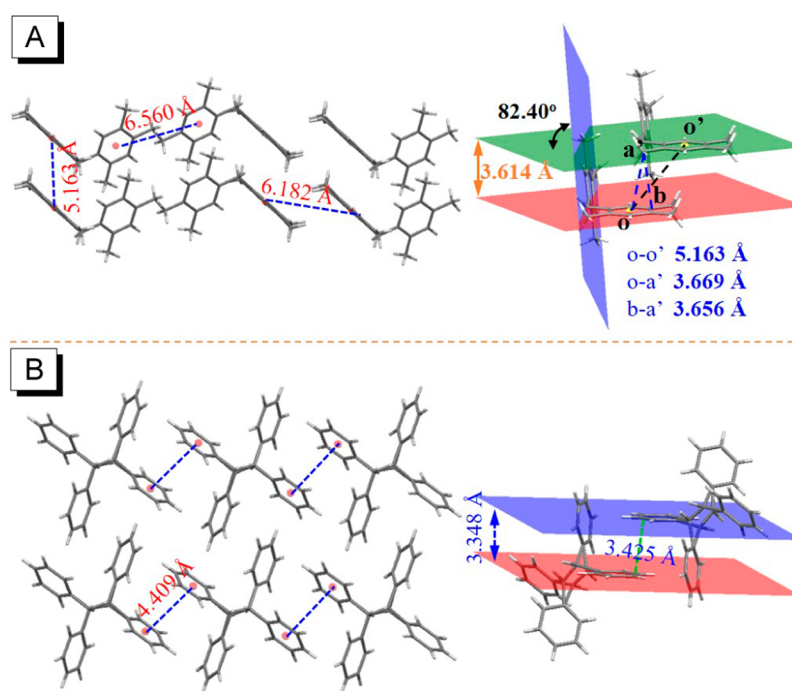


**Figure 7.** Crystal packing diagrams of (A) DPM and (B) *s*-TPE.

suggest that their chromophoric units were 1,2,4-trimethylbenzene and benzene, which could be excited by UV light at 250–280 nm. However, chromophores with longer-wavelength emission and excitation could not be easily identified. They should be generated through some inter- or intramolecular interactions. Meanwhile, all of the present molecules showed typical AIE characteristic in THF/water mixture even at the longer-excitation wavelength (Figures 6, S11, and S12). For example, as depicted in Figure 6, *s*-TPE showed longer-range with  $\lambda_{em}$  of 460 nm and demonstrated AIE characteristic at  $\lambda_{ex}$  = 280 and 340 nm. The difference between the two spectra was that there was no shorter-wavelength emission at 290 nm at  $\lambda_{ex}$  = 340 nm.

**2.3. Crystal Structures.** The distance and dihedral angle between different atoms and planes in their crystal structures were measured to demonstrate the inter- or intramolecular interaction. In DPM, the dihedral angle between two intramolecular benzene rings was 82.40° (Figure 7A). Its dimer structure showed that the two intermolecular benzene

rings were parallel to each other. While the interplanar distance was 3.614 Å and the centroid *o* to centroid *o'* was 5.163 Å, the distances between carbon *a'* and *b*, *a'* and centroid *o* were 3.656 and 3.669 Å, respectively. These data suggested that DPM showed weak intermolecular interaction. Similarly, crystal structure analysis of *s*-TPE-TM also suggested minor intermolecular interaction (Figure S13), possibly due to the steric hindrance introduced by the methyl groups.

Due to the absence of methyl group, *s*-TPE showed tighter packing than other molecules. Each molecule formed two pairs of intermolecular cofacial packing with their adjacent benzene rings (Figure 7B). The centroid–centroid distance was 4.409 Å, and the vertical distance between two benzene planes was 3.348 Å. The shortest C–C distance was 3.425 Å, which was short enough to generate weak intermolecular interaction. Thus, one question arises: does this weak intermolecular–stacking in *s*-TPE lead to the broad emission with  $\lambda_{em}$  = 467 nm and high quantum yield in the solid state?

**Table 2. Energy Levels, Energy Gaps, Calculated Absorption, and Emission Maximum of TMB, DPM, *s*-TPE-TM, and *s*-TPE Calculated by the TD-DFT, B3LYP/6-31G(d), and Gaussian 09 Program<sup>a</sup>**

compound	HOMO (eV)		LUMO (eV)		energy gap (eV)		$\lambda_{\text{abs}}$ (nm)	$\lambda_{\text{em}}$ (nm)
	GS	ES	GS	ES	GS	ES		
TMB	-5.907	-5.890	0.428	0.019	6.335	5.909	231	251
DPM	-5.727	-5.711	0.486	0.052	6.213	5.763	234	253
<i>s</i> -TPE-TM	-5.454	-5.322	0.148	-0.358	5.602	4.964	247	281
<i>s</i> -TPE	-5.978	-4.845	-0.060	-1.406	5.918	3.439	236	462

<sup>a</sup>Abbreviation: HOMO = highest occupied molecular orbitals, LUMO = lowest unoccupied molecular orbitals, GS = ground state, ES = excited state,  $\lambda_{\text{abs}}$  = absorption maximum,  $\lambda_{\text{em}}$  = emission maximum.

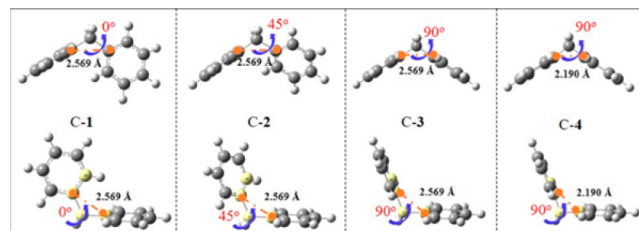
**2.4. Through-Space Interaction.** To answer the above question, simulation on these three molecules was carried out. According to the dimer simulation based on their crystal structures (Tables S2–S4),<sup>30–33</sup> the exciton coupling energy for all the dimers of the crystals were merely around 1 meV. This value was much lower than those (around 200 meV) of the system with strong packing<sup>34</sup> suggesting that the longer-wavelength emission in the aggregate of the single bond-bridged AIEgens was predominantly ascribed to intramolecular rather than intermolecular interaction. Single molecule simulation in the gas phase was then conducted, treating the crystal structures of the molecules as the ground-state configuration. The TD-DFT calculation with B3LYP/6-31G(d) was utilized to simulate the ground- and excited-state frontier molecular orbitals (Table 2 and Figure S14), including the electron cloud distribution and energy levels of highest occupied molecular orbitals (HOMO) and lowest unoccupied molecular orbitals (LUMO). According to the experimental UV and PL data (Table 1), the  $\lambda_{\text{abs}}$  and the PL peak at 300 nm of DPM, *s*-TPE-TM, and *s*-TPE corresponded to the absorption and emission of a single phenyl ring.<sup>18</sup> The calculated  $\lambda_{\text{abs}}$  of DPM, *s*-TPE-TM, and *s*-TPE was similar to TMB, demonstrating their nonconjugated ground-state structures (Table 2).

Simulation in the excited state was further carried out as it had a direct relationship with the PL property. According to the previous researches on diphenylmethane, homoconjugation between these two methylene-linked benzene rings existed, which induced effective electron delocalization and overlapping between benzene rings.<sup>35,36</sup> As shown in Figure S14A, the LUMO electron cloud of DPM spread on the whole molecule, revealing that the two phenyl rings were electronically conjugated. Alternatively, it was found that the homoconjugation of diphenylmethane had a close relationship with the twisting angle and the distance between the benzene rings. Generally, the homoconjugation was favored when the phenyl rings were close to each other and packed in a parallel fashion, as suggested by the comparing results between compound C-1 to C-4 in Table 3. With an increase in the twisting angle from conformer C1 to C3, the energy gap slightly decreased from 6.239 to 6.214 eV. Further shortening the distance between phenyl rings C3 and C4 from 2.569 to 2.190 Å decreased the energy gap obviously to 5.704 eV. Additionally, the broad emission of DPM in the aggregate state was caused by different conformers. As each conformer had its specific emission wavelength, this explained why DPM exhibited excitation-dependent emission. Theoretically, the emission will be located at the longer-wavelength region with an increase in homoconjugation. However, the calculated  $\lambda_{\text{em}}$  for DPM was 253 nm and was similar to TMB and its solution value. Why the simulation result deviated from the experimental result was that the simulation was carried out in the gas phase. Thus, the two

**Table 3. Energy Levels, Energy Gaps in the Ground State, Calculated Maximum Absorption of Diphenylmethanes C1–C4 with Different Twisting Angles and C–C Distances Calculated by the TD-DFT, B3LYP/6-31G(d), Gaussian 09 Program<sup>a,b</sup>**

compound	HOMO (eV)	LUMO (eV)	Energy gap (eV)	$\lambda_{\text{abs}}$ (nm)
C-1	-6.357	-0.118	6.239	230
C-2	-6.311	-0.076	6.235	231
C-3	-6.294	-0.08	6.214	233
C-4	-5.911	-0.207	5.704	249

<sup>a</sup>Abbreviation: HOMO = highest occupied molecular orbitals, LUMO = lowest unoccupied molecular orbitals,  $\lambda_{\text{abs}}$  = absorption maximum. <sup>b</sup>



benzene rings could undergo free rotation in the absence of strong steric hindrance. Molecular optimization in the excited state showed that the two benzene rings were almost perpendicular to each other (Figure S14A). Since the orthogonal structure of diphenylmethane corresponded to the worst through-space conjugation and largest energy gap, the calculated  $\lambda_{\text{em}}$  will be bathochromically shifted once the rigidity of single molecule increased. This could be verified by the simulation results on *s*-TPE-TM and *s*-TPE.

The simulated  $\lambda_{\text{em}}$  of *s*-TPE-TM in the ground state was 281 nm, which was 30 nm red shifted from that of DPM (Table 1). This suggested that the four phenyl rings were not totally isolated, and they interacted intramolecularly in a through-space manner.<sup>35–39</sup> As observed from its LUMO, there was overlapping between phenyl ring electrons through the methylene bridge (Figures 8 and S14B). However, Table 4 showed that the distance between atom 1 and 4 became longer in the excited state and the electron clouds of the associated phenyl rings (B1 and B4) were no longer overlapped. This resulted in a large similarity in emission maximum and UV spectrum between *s*-TPE-TM and DPM in the aggregate state, and also proved that the through-space conjugation between phenyl rings B1 and B2, and B3 and B4 played the predominated role in its optical property. The interaction between B2 and B3 or B1 and B4 should make little contribution. Because *s*-TPE-TM possessed a crowded structure to impart stronger molecular rigidity, that might account why the calculated  $\lambda_{\text{em}}$  of *s*-TPE-TM was 30 nm longer than DPM. The absence of orthogonal structure between

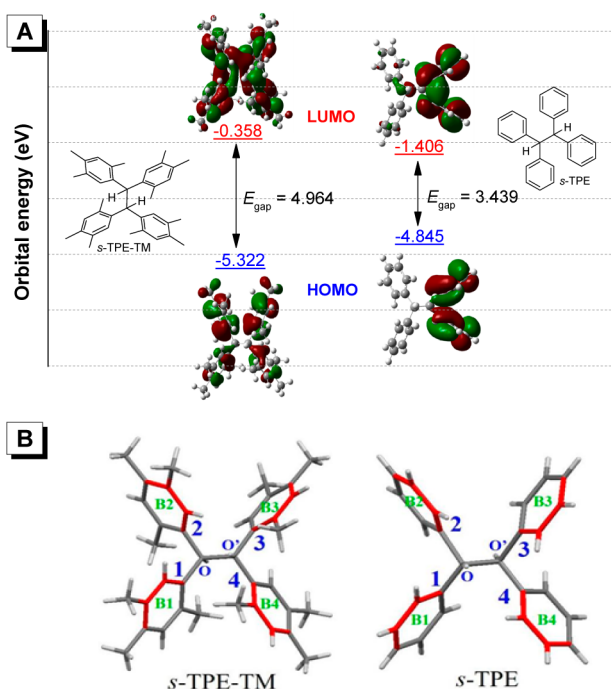


**Figure 8.** (A) Electron cloud distributions, energy levels of *s*-TPE-TM and *s*-TPE in the excited state calculated by TD-DFT B3LYP/6-31G(d), Gaussian 09 program. (B) Schematic definition of carbon atoms and phenyl rings in *s*-TPE-TM and *s*-TPE.

phenyl rings B1 and B2, and B3 and B4 could induce better through-space conjugation to narrow the band gap.

The simulation results of *s*-TPE were correlated with the experimental data (Table 1). For example, the calculated  $\lambda_{em}$  was 462 nm, which was equal to the experimental one (460 nm). Table 4 showed that the twisting angle of phenyl rings B3 and B4 in *s*-TPE synchronously increased to  $\sim 90^\circ$  in the excited state and the distance between atoms 3 and 4 decreased to 2.159 Å, forming an almost cofacial dimer structure. This structure was demonstrated by the fact that the electron clouds of the associated phenyl rings (B3 and B4) were delocalized in the excited state (Figure 8A). These data suggested that the through-space conjugation between phenyl rings B3 and B4 made the greatest contribution to the longer-wavelength emission in *s*-TPE. The single bond in *s*-TPE also played an important role to promote the through-space conjugation as it provided flexibility for the benzene rings to rotate. The absence of methyl groups on the benzene rings decreased their steric interaction, making them to get closer with little constraint.

Photoluminescence quantum efficiency ( $\eta_{pl}$ ) was determined by the radiative ( $k_r$ ) and nonradiative ( $k_{nr}$ ) decay rate of the singlet excite. According to the equations  $\eta_{pl} = \frac{k_r}{k_r + k_{nr}}$  and  $k_r = f\Delta E^2/1.5$ , where  $f$  is the dimensionless oscillator strength, and  $\Delta E$  is the vertical transition energy.  $k_{nr}$  consists of two contributions: (i) the internal conversion  $k_{IC}$  from S1 to S0 and (ii) the intersystem crossing  $k_{ISC}$  from S1 to T1. In fluorescent AIE system,  $\eta_{pl}$  was approximately proportional to the oscillator strength ( $f$ ) and inversely proportional to the reorganization energy ( $\lambda$ ).<sup>40,41</sup> Then, these two factors were calculated for *s*-TPE in both gas phase and crystal state. The oscillator strength for the electronic transition from S1 to S0 state of *s*-TPE in the gas phase was only 0.0036. Figure 9A showed the reorganization energy at different wavenumbers in gas phase.

**Table 4. Calculated C–C Distances and Twisting Angle of *s*-TPE-TM and *s*-TPE in the Ground (GS) and Excited (ES) States Calculated by the TD-DFT, B3LYP/6-31G(d), Gaussian 09 Program<sup>a</sup>**

compound	ground state				excited state			
	atomic distance (Å)	3–4	4–1	twist angle (deg)	atomic distance (Å)	3–4	4–1	twist angle (deg)
<i>s</i> -TPE-TM	2.508	3.018	2.519	3.047	70.93	71.59	78.17	65.66
<i>s</i> -TPE	2.507	3.015	2.507	3.015	77.34	79.51	61.29	63.99
						2.159	3.094	88.64
						2.491	3.262	86.38

<sup>a</sup>Set (1–2–O') as the reference plane when calculated the twisting angle of phenyl rings B1 and B2. Set (3–4–O) as the reference plane when calculated the twisting angle of phenyl rings B3 and B4.

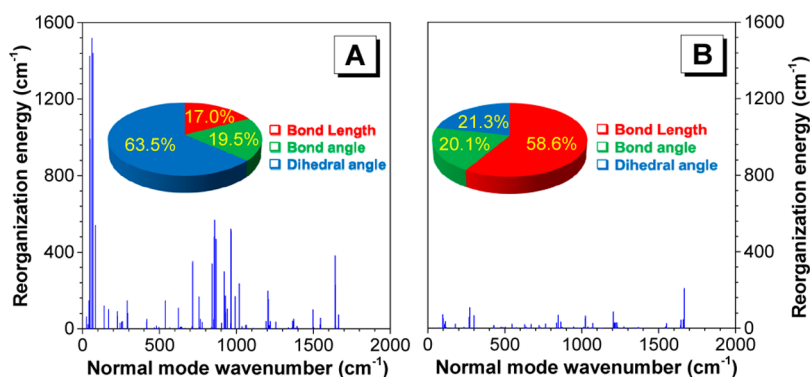


**Figure 9.** Plots of calculated reorganization energy versus the normal mode wavenumber of *s*-TPE in (A) gas phase and (B) crystal. Calculated by the TD-DFT, B3LYP/6-31G(d), and Gaussian 09 program.

The total  $\lambda$  was as high as 15 483  $\text{cm}^{-1}$  and 63.5% of them was contributed to the change of dihedral angle caused by the rotation of phenyl rings. The small oscillator strength and large reorganization energy led to weak emission at the longer wavelength in the solution state. The aggregation effect was modeled through a combined quantum mechanics and molecular mechanics (QM/MM) approach using Gaussian 09 package. A cluster containing 73 molecules cut from the single crystal structure set up the two-layer oniom model. The central molecule acted as the high layer (QM) at the (TD)B3LYP/6-31G(d) level, and the surrounding ones were treated as the low layer (MM) using Universal Force Field (UFF). First, the low layer was fixed and only the central molecule was optimized by the (TD)B3LYP/6-31G(d). The calculated oscillator strength enormously increased to 0.1259 which was 35-times larger than that in the gas phase. Meanwhile, its total  $\lambda$  sharply decreased to 1712  $\text{cm}^{-1}$  and 58.6% of them was contributed to the change of bond length (Figure 9B). The large oscillator strength and small reorganization energy in the QM/MM calculation could help to elucidate the bright fluorescent emission in the solid state. However, the calculated S1–S0 emission wavelength was only 255 nm, which was quite bluer than the calculated  $\lambda_{\text{em}} = 462$  nm in the gas phase. The deviation of calculated  $\lambda_{\text{em}}$  could be ascribed to the fixed surrounding environment, the narrow space and steric hindrance restricted the centrally molecular motion and prevented the central molecule from forming the through-space conjugation. Then, another type of oniom calculation was performed by making the low layer optimized at the MM level in order to evaluate different constrain effect on the QM molecule caused by the MM part. Indeed, the calculated  $\lambda_{\text{em}}$  was bathochromic-shift to 277 nm. Meanwhile, reorganization energy increased to 3314  $\text{cm}^{-1}$ , Figure S15 showed that the percentage of dihedral angle-change contribution to the reorganization energy increased from 21.3% (fixed low layer mode) to 37.8% (active low layer mode), which was more favorable to form the intramolecular through-space conjugation. As the limit of theoretical calculation in nonconventional systems, more advanced calculation methods and accurate modes still need to be developed and constructed to support the solid-state through-space conjugation.

Another interesting phenomenon was that their UV spectra only showed peaks associated with the absorption of 1,2,4-trimethylbenzene or benzene. Even no through-space conjugation peaks were observed in their absorption spectra, these molecules could still be excited by light with wavelength longer than their UV cutoff and phenyl emission. For example, the UV

cutoff wavelength of *s*-TPE was 275 nm (Figure SSC) and the emission tail of benzene was located at 330 nm (Figure 3A). However, *s*-TPE could still be excited by light at 340 nm in THF/water mixtures (Figure 6). According to the previous research on through-space interaction,  $\pi-\pi^*$  transition stemmed from through-space interaction was normally not observed because it is forbidden in the ground state.<sup>37</sup> The calculated wavelength and oscillator strength of diphenylmethanes C1–C4 with different twisting angles and C–C distances could support this mechanism (Table S5). Among these four structures, C-4 possessed the longest wavelength (S1–S0 electronic transition) which indicated the strongest through-space interaction. However, its oscillator strength was merely 0.0006, which was the reason why this peak could not be detected in its absorption spectrum.

### 3. CONCLUSIONS

In this work, three nonconjugated compounds were synthesized by linking isolated phenyl rings with alkyl group. While their UV spectra exhibited peaks related to the absorption of isolated phenyl rings, their PL spectra in the aggregate state showed emission from phenyl or 1,2,4-trimethylphenyl ring and chromophore formed by through-space interaction between methylene-linked phenyl rings. These molecules could be excited by longer-wavelength UV light and showed excitation-dependent emission. The longer-wavelength emission induced by through-space interaction was only observed in the aggregate state due to the RIR mechanism. High quantum yield of up to 69% would be reached in the solid state. The simulated results were consisted with the experimental results and supported the existence of through-space conjugation in these molecules. These alkyl-linked arenes broadened the type of fluorophore and suggested that traditional conjugated structures were not necessary for generating efficient light emission. Nonconventional systems, such as clusteroluminogens,<sup>42,43</sup> could also emit fluorescence in the visible range with high fluorescence quantum yield.

### ■ ASSOCIATED CONTENT

#### Supporting Information

The Supporting Information is available free of charge on the ACS Publications website at DOI: 10.1021/jacs.7b08592.

- Details of the chemicals, instrumentation, synthesis, and characterization (PDF)
- Crystallographic structure (CIF)
- Crystallographic structure (CIF)

Crystallographic structure (CIF)

## ■ AUTHOR INFORMATION

## Corresponding Author

\*tangbenz@ust.hk

ORCID 

Haoke Zhang: 0000-0001-7309-2506

Nelson L. C. Leung: 0000-0003-3949-9622

Xuhui Huang: 0000-0002-7119-9358

Ryan T. K. Kwok: 0000-0002-6866-3877

Anjun Qin: 0000-0001-7158-1808

Ben Zhong Tang: 0000-0002-0293-964X

## Notes

The authors declare no competing financial interest.

## ■ ACKNOWLEDGMENTS

This work was partially supported by the National Basic Research Program of China (973 Program; 2013CB834701 and 2013CB834702), the University Grants Committee of Hong Kong (AoE/P-03/08), the Research Grants Council of Hong Kong (16301614, 16305015, C2014-15G, A-HKUST605116, and N\_HKUST604/14), and the Innovation and Technology Commission (ITC-CNERC14SC01 and TCPD/17-9). B.Z.T. is also grateful for the support from the Guangdong Innovative Research Team Program of China (201101C0105067115), the Science and Technology Plan of Shenzhen (JCYJ 20160229205601482), and the Shenzhen Peacock Plan.

## ■ REFERENCES

- (1) Stelzer, E. H. K. *Nat. Methods* **2014**, *12*, 23.
- (2) Loizzo, M. R.; Tundis, R.; Conforti, F.; Statti, G. A.; Menichini, F. *Pharm. Biol.* **2009**, *47*, 516.
- (3) Tang, C. W.; VanSlyke, S. A. *Appl. Phys. Lett.* **1987**, *51*, 913.
- (4) Chen, L.; Nakamura, M.; Schindler, T. D.; Parker, D.; Bryant, Z. *Nat. Nanotechnol.* **2012**, *7*, 252.
- (5) Zhao, Z. J.; Lam, J. W. Y.; Tang, B. Z. *Soft Matter* **2013**, *9*, 4564.
- (6) Aubin, J. E. J. *Histochem. Cytochem.* **1979**, *27*, 36.
- (7) Zhang, W. F.; Guo, H.; Ma, G. H.; Huang, Y. B.; Du, Z. L. *Chin. Phys. Lett.* **1998**, *15*, 591.
- (8) Yanari, S. S.; Bovey, F. A.; Lumry, R. *Nature* **1963**, *200*, 242.
- (9) Ye, R. Q.; Liu, Y. Y.; Zhang, H. K.; Su, H. F.; Zhang, Y. L.; Xu, L. G.; Hu, R. R.; Kwok, R. T. K.; Wong, K. S.; Lam, J. W. Y.; Goddard, W. A.; Tang, B. Z. *Polym. Chem.* **2017**, *8*, 1722.
- (10) Hirayama, F. *J. Chem. Phys.* **1965**, *42*, 3163.
- (11) Birks, J. B. *Photophysics of Aromatic Molecules*; Wiley-Interscience: London, 1970.
- (12) Zhao, Z. J.; Chen, S. M.; Lam, J. W. Y.; Wang, Z. M.; Lu, P.; Mahtab, F.; Sung, H. H. Y.; Williams, I. D.; Ma, Y. G.; Kwok, H. S.; Tang, B. Z. *J. Mater. Chem.* **2011**, *21*, 7210.
- (13) Kim, Y.; Bouffard, J.; Kooi, S. E.; Swager, T. M. *J. Am. Chem. Soc.* **2005**, *127*, 13726.
- (14) Mei, J.; Leung, N. L.; Kwok, R. T.; Lam, J. W.; Tang, B. Z. *Chem. Rev.* **2015**, *115*, 11718.
- (15) Nie, H.; Hu, K.; Cai, Y. J.; Peng, Q.; Zhao, Z. J.; Hu, R. R.; Chen, J. W.; Su, S. J.; Qin, A. J.; Tang, B. Z. *Mater. Chem. Front.* **2017**, *1*, 1125.
- (16) Luo, J. D.; Xie, Z. L.; Lam, J. W. Y.; Cheng, L.; Chen, H. Y.; Qiu, C. F.; Kwok, H. S.; Zhan, X. W.; Liu, Y. Q.; Zhu, D. B.; Tang, B. Z. *Chem. Commun.* **2001**, 1740.
- (17) Chen, L.; Lin, G. W.; Peng, H. R.; Ding, S. Y.; Luo, W. W.; Hu, R. R.; Chen, S. M.; Huang, F.; Qin, A. J.; Zhao, Z. J.; Tang, B. Z. *Mater. Chem. Front.* **2017**, *1*, 176.
- (18) <http://webbook.nist.gov/cgi/cbook.cgi?Spec=C95636&Index=0&Type=UVVis&Large=on&SVG=on>.
- (19) <http://omlc.org/spectra/PhotochemCAD/html/042.html>.
- (20) Hong, Y. N.; Lam, J. W. Y.; Tang, B. Z. *Chem. Soc. Rev.* **2011**, *40*, 5361.
- (21) Li, J.; Yang, C.; Huang, C.; Wan, Y.; Lai, W. Y. *Tetrahedron Lett.* **2016**, *57*, 1256.
- (22) Krukowski, P.; Tsuzuki, T.; Minagawa, Y.; Yajima, N.; Chaunchaiyakul, S.; Akai-Kasaya, M.; Saito, A.; Miyake, Y.; Katayama, M.; Kuwahara, Y. *J. Phys. Chem. C* **2016**, *120*, 3964.
- (23) Pross, A.; Radom, L.; Riggs, N. V. *J. Am. Chem. Soc.* **1980**, *102*, 2253.
- (24) Alabugin, I. V.; Gilmore, K. M.; Peterson, P. W. *Comput. Mol. Sci.* **2011**, *1*, 109.
- (25) Karpovich, D. S.; Blanchard, G. J. *J. Phys. Chem.* **1995**, *99*, 3951.
- (26) Lakowicz, J. R. *Principles of Fluorescence Spectroscopy*; Springer Science+Business Media: New York, 2006.
- (27) Cushing, S. K.; Li, M.; Huang, F. Q.; Wu, N. Q. *ACS Nano* **2014**, *8*, 1002.
- (28) Lee, K. M.; Cheng, W. Y.; Chen, C. Y.; Shyue, J. J.; Nieh, C. C.; Chou, C. F.; Lee, J. R.; Lee, Y. Y.; Cheng, C. Y.; Chang, S. Y.; Yang, T. C.; Cheng, M. C.; Lin, B. Y. *Nat. Commun.* **2013**, *4*, 1544.
- (29) Qian, H.; Cousins, M. E.; Horak, E. H.; Wakefield, A.; Liptak, M. D.; Aprahamian, I. *Nat. Chem.* **2016**, *9*, 83.
- (30) Li, W. Q.; Peng, Q.; Xie, Y. J.; Zhang, T.; Shuai, Z. G. *Huaxue Xuebao* **2016**, *74*, 902.
- (31) Hsu, C. P.; You, Z. Q.; Chen, H. C. *J. Phys. Chem. C* **2008**, *112*, 1204.
- (32) <http://www.shuaigroup.net/index.php>.
- (33) Valiev, M.; Bylaska, E. J.; Govind, N.; Kowalski, K.; Straatsma, T. P.; Van Dam, H. J. J.; Wang, D.; Nieplocha, J.; Apra, E.; Windus, T. L.; de Jong, W. A. *Comput. Phys. Commun.* **2010**, *181*, 1477.
- (34) Plötz, P. A. Master's Thesis; University of Rostock: Mecklenburg-Vorpommern, Germany, 2013.
- (35) Martinez, A. G.; Barcina, J. O.; Cerezo, A. F.; Rivas, R. G. *J. Am. Chem. Soc.* **1998**, *120*, 673.
- (36) Caraballo-Martinez, N.; Heras, M. d. R. C.; Blazquez, M. M.; Barcina, J. O.; Martinez, A. G.; Salvador, M. d. R. T. *Org. Lett.* **2007**, *9*, 2943.
- (37) Hoffmann, R. *Acc. Chem. Res.* **1971**, *4*, 1.
- (38) Chen, L.; Wang, Y. H.; He, B. R.; Nie, H.; Hu, R. R.; Huang, F.; Qin, A. J.; Zhou, X. S.; Zhao, Z. J.; Tang, B. Z. *Angew. Chem., Int. Ed.* **2015**, *54*, 4231.
- (39) Zhang, Y. Y.; He, B. R.; Luo, W. W.; Peng, H. R.; Chen, S. M.; Hu, R. R.; Qin, A. J.; Zhao, Z. J.; Tang, B. Z. *J. Mater. Chem. C* **2016**, *4*, 9316.
- (40) Shuai, Z.; Peng, Q. *Natl. Sci. Rev.* **2016**, *4*, 224.
- (41) Zhang, T.; Jiang, Y.; Niu, Y.; Wang, D.; Peng, Q.; Shuai, Z. *J. Phys. Chem. A* **2014**, *118*, 9094.
- (42) Viglianti, L.; Leung, L. C.; Xie, N.; Gu, X.; Sung, H. Y.; Miao, Q.; Williams, I. D.; Licandro, E.; Tang, B. Z. *Chem. Sci.* **2017**, *8*, 2629.
- (43) Zhou, X.; Luo, W.; Nie, H.; Xu, L.; Hu, R.; Zhao, Z.; Qin, A.; Tang, B. Z. *J. Mater. Chem. C* **2017**, *5*, 4775.